Journal of Ceramic Processing Research. Vol. 22, No. 6, pp. 615~619 (2021)
(Received 3 March 2021, Received in revised form 14 May 2021, Accepted 3 June 2021)
https://doi.org/10.36410/jcpr.2021.22.6.615

J O U R N A L O F
Ceramic Processing Research

Improving electrochemical characteristics of Ni-rich cathode materials by Na doping

Do-Young Hwang and Seung-Hwan Lee*
Department of Advanced Materials Engineering, Daejeon University, Daejeon 34520, Republic of Korea

In this paper, we successfully synthesized the Na-doped Ni-rich $LiNi_{0.8}Co_{0.1}Mn_{0.1}O_2$ cathode by a general co-precipitation. We investigated the influence of Na doping in terms of structural characteristics and electrochemical performances for practical usage of lithium-ion batteries. Particularly, the Na-doped Ni-rich $LiNi_{0.8}Co_{0.1}Mn_{0.1}O_2$ cathode shows a significant improvement in cyclability of 72.7 % after 80 cycles with no morphology change, compared to the pristine NCM. Therefore, we can conclude that Na-doped Ni-rich $LiNi_{0.8}Co_{0.1}Mn_{0.1}O_2$ can be considered as an effective strategy for state-of-the-art lithium-ion batteries.

Keywords: Ni-rich layered structure, Na-doped $LiNi_{0.8}Co_{0.1}Mn_{0.1}O_2$, enhanced electrochemical performances, superior structural stability, next-generation Li-ion batteries.

Introduction

Lithium-ion batteries (LIBs) have used as the main power source for various applications including electric vehicles, hybrid electric vehicles and uninterruptible power supplies due to their various merits like extraordinary energy density, long cycle life and excellent stability [1, 2]. Recently, ternary layer structured $LiNi_xCo_yMn_zO_2$ (NCM, $0 \le x, y, z < 1$) cathode materials have received widespread attention for commercial applications [3]. Among the family of NCM cathode, Ni-rich NCM ($x \ge 80\%$) cathodes have intensively researched for next-generation LIBs because of higher Ni content contributes to cost-effectiveness, high practical capacity and low toxicity compared to traditional cathodes [3, 4]. However, the Ni-rich cathodes of inherent issues such as safety problems and inferior capacity retention hinder its commercialization [5].

In order to overcome these defects, surface coating and bulk doping are commonly employed to improve structural stability and electrochemical performance [1]. Surface coating, such as SiO_2 [1], TiO_2 [2], ZrO_2 [6] and carbon [7], is an attractive approach to accomplish the superior cycle and rate performance of Ni-rich NCM cathode materials. The surface coated layer over the cathode suppresses direct contact with the electrolyte and reduces undesirable side reactions [8]. The other approach to improve the electrochemical performance of Ni-rich cathode is bulk doping with Ce [9], Al [10], Mg [11], Na [12] and so on. Furthermore, the introduction of bulk doping causes rapid Li^+ ion diffusion into the electrode and enhancing structural stability due to increased Li slab spacing [13].

Therefore, in this work, we synthesized a well-crystallized Na-doped $LiNi_{0.8}Co_{0.1}Mn_{0.1}O_2$ via a co-precipitation method to improve electrochemical performance.

Experimental

The sphere-like NCM cathode was prepared using the general co-precipitation method. A proper amount of four solutes like $NiSO_4 \cdot 6H_2O$, $CoSO_4 \cdot 7H_2O$, $MnSO_4 \cdot H_2O$, Na_2CO_3 and $NH_3 \cdot H_2O$ were served as the starting materials to yield precursor $Ni_{0.8}Co_{0.1}Mn_{0.1}(OH)_2$. Simultaneously, NaOH and NH_4OH were employed as chelating agents. The obtained precursor $Ni_{0.8}Co_{0.1}Mn_{0.1}(OH)_2$ was uniformly mixed with $LiOH \cdot H_2O$ via a molar ratio of 1:1.05 to prepare the pristine NCM. Afterward, the as-prepared mixture was sintered at 500 °C for 6 h, 780 °C for 15 h and then cooling the resulting sample under room temperature. In order to prepare the Na-doped $LiNi_{0.8}Co_{0.1}Mn_{0.1}O_2$ (N-NCM) cathode, the same synthesis process above was conducted by replacing Li_2CO_3 with Li_2CO_3 and Na_2CO_3 mixture (with a molar ratio of 97:3).

The cathode was prepared by coating a slurry using an active material powder, carbon black and polyvinylidene fluoride with 96:2:2 mass ratio, and subsequently 1-metal-2-pyrrolidinone (NMP) solvent was added to obtain slurry onto an Al foil. Then, this electrode was heated in a oven at 130 °C for 10 h. The coin cell assembled with a resulting positive electrode, lithium metal as an anode, a porous polypropylene film as a separator. Finally, 1M lithium hexafluorophosphate ($LiPF_6$) dissolved in the organic solvents from ethylene carbonate (EC)/dimethyl carbonate (DMC)/ethyl-methyl

*Corresponding author:
Tel : +82-42-280-2414
E-mail: shlee@dju.kr

carbonate (EMC) for an electrolyte in a volumetric ratio of 1:1:1.

The X-ray diffraction (Philips, X-pert PRO MPD) measurement was tested to investigate the structural characteristics of the samples with Cu-Kα radiation in the 2θ from 10° to 70°. The field emission scanning electron microscopy (FE-SEM, Hitachi S-4800) was served to evaluate particle morphology with EDS mapping system. Also, cross-sectioned FE-SEM images are obtained by Focused ion beam (FIB). The electrochemical performances were conducted out using measurement equipment (TOSCAT-3100, Toyo system). Different current densities are evaluated by an electrochemical machine (TOCAT-3100, Toyo system).

Results and Discussion

Fig. 1 exhibits the XRD tests of the pristine NCM and N-NCM samples in the range of 10°-80°. All diffraction patterns are represented as a layered hexagonal α-$NaFeO_2$ structure corresponding to the space group $R\bar{3}m$ without any additional impurity peaks [14]. It can be explained that Na^+ doping process does not affect the original bulk structure of layered NCM owing to low doping concentration [15]. From both XRD patterns, it is clear that there are two distinct splits of (006)/(102) and (108)/(110) peaks, suggesting that samples are synthesized with a well-ordered crystal structure [16]. Particularly, as displayed in Fig. 1(b), the (003) peak of N-NCM shows a leftward shift in the axis of 2θ by comparison with the pristine NCM, inferring that sodium ion is successfully substituted with lithium-ion in the N-NCM cathode. Besides, it can be speculated that the incorporation of Na^+ contributes to enlarged Li slab spacing and stabilizes the structure with fast lithium-ion diffusion owing to larger ionic radii (1.02 Å) than Li^+ (0.76 Å), Co^{3+} (0.54 Å) and Mn^{4+} (0.53 Å) [3]. Also, the I(003)/I(104) intensity ratio is closely relative to Li^+/Ni^{2+} cation disorder, which is resulted from the similar size of the ionic radius of Li^+ (0.76 Å) and Ni^{2+} (0.69 Å) at the 3a site [17, 18]. As for N-NCM, I(003)/I(104) intensity ratio is 1.54, which is much larger than the standard value (1.2) for cation disorder. As a result, we can conclude that surface modification by sodium substitution can suppress the Li^+/Ni^{2+} cation disorder with a well-defined layered structure.

Fig. 2 exhibits FE-SEM images of pristine NCM and P-NCM samples. It can be observed that all cathode materials are composed of sphere-like morphology with an average primary particle size of approximately 9.7 μm. Moreover, the spherical secondary particles consist of primary particles of about 175 nm. Here, there are no big differences between the surface morphology of the pristine NCM (Fig. 2(a)) and N-NCM (Fig. 2(b)). This observation indicates that sodium doping does not change the sphere-like morphology as well as the particle size of NCM cathode materials. Fig. 2(c) shows EDS mapping images of N-NCM to observe the existence of Na atom. We can observe that Ni, Co, Mn and Na atoms are uniformly distributed in N-NCM sample.

In the case of electrochemical tests, the loading level of active materials was prepared about 14.6 mg cm^{-2} to meet a condition of practical use for LIBs [19]. Fig. 3 shows the long-term cycle performance of the pristine NCM and N-NCM at a rate of 1 C in 3.0-4.3 V at 25 °C. We can also evaluate the initial discharge at the 1st cycle, showing that N-NCM (202.1 mAh g-1) has slightly higher than the pristine NCM (194.3 mAh g^{-1}). Compared to the pristine NCM, N-NCM sample exhibits a better capacity owing to its rapid electrode kinetics and high material utilization. Also, it could be originated from high content of cation mixing [20]. Furthermore, the improvement in electrochemical performance by the introduction of sodium doping is more clearly presented by the cycle test. From Fig. 3, N-NCM exhibits superior life-span cyclic stability with 72.7% after 80 cycles compared to that of pristine NCM (60.0%). The inferior cycling performance of the pristine NCM is due to the migration of Ni^+ to the Li layer during cycling, leading to not only the layered structure deformation, but also rapid capacity fading of NCM cathode materials [21, 22]. The pristine NCM also suffers from the generation of microcracks, deriving from abrupt lattice

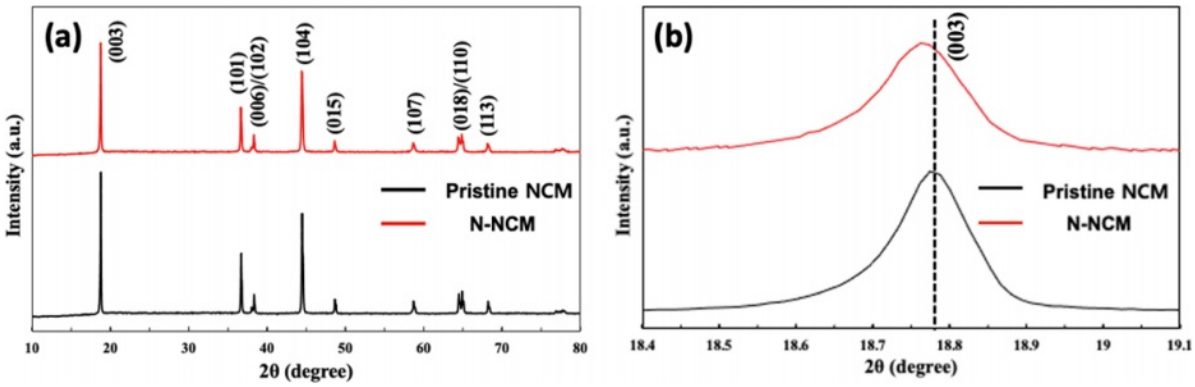

Fig. 1. (a) XRD pattern of pristine NCM and N-NCM, (b) (003) diffraction peak of samples.

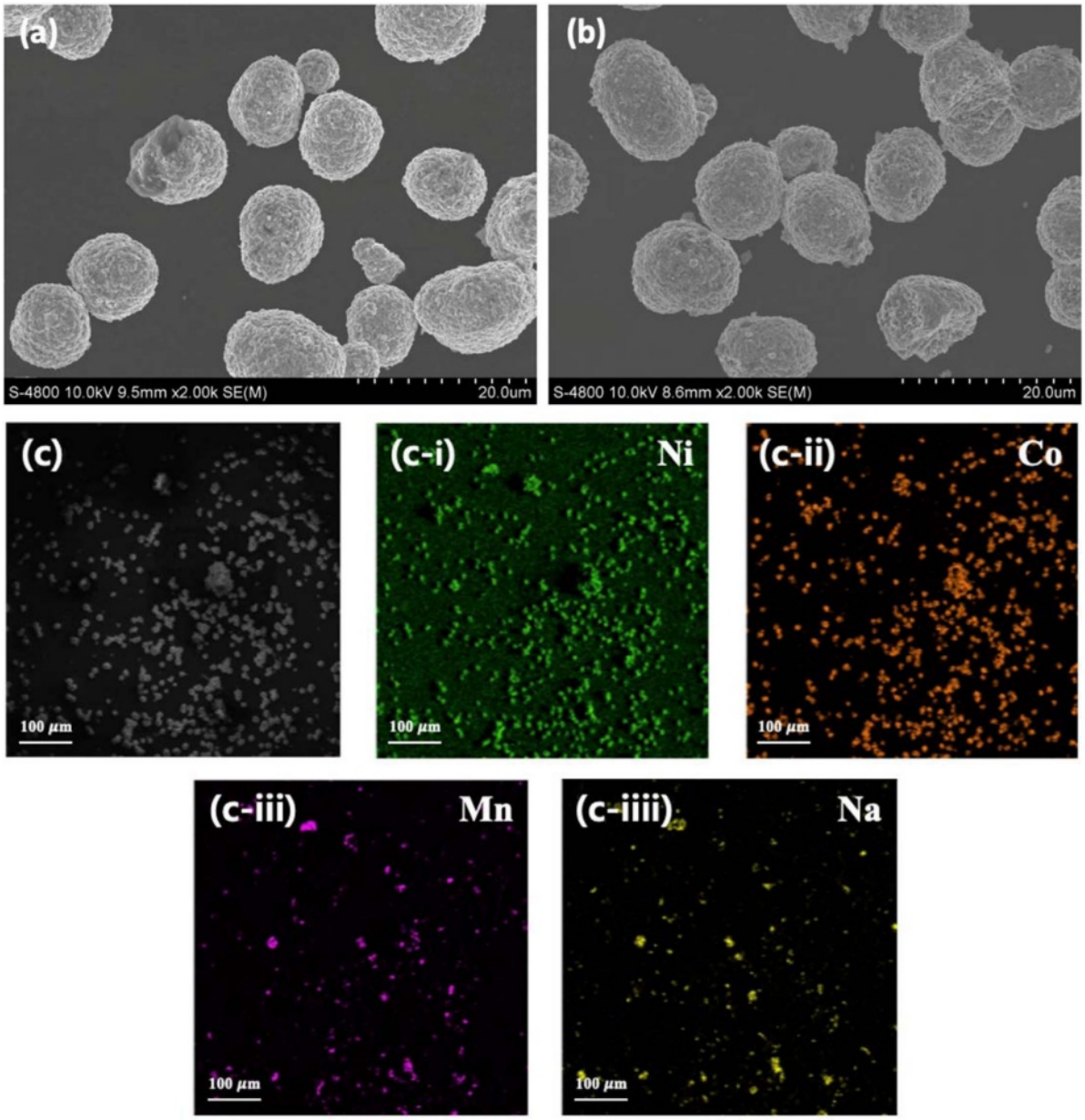

Fig. 2. FE-SEM images of (a) pristine NCM, (b) N-NCM and (c) EDS mapping images of N-NCM.

change during long-term cycling. More importantly, these cracks become pathways for the electrolyte infiltration and block Li^+ ion transport by forming the solid electrolyte interface (SEI) layer over the cathode surface [2]. However, as for N-NCM, the improved cycling performance is attributed to the incorporation of Na^+ into the layered structure, which can effectively suppress fast capacity fading and decay of the Li layer with large radiuses owing to the "pillar effect" [23]. Thus, the Na^+ as a pillar ion can shield the O^{2-}-O^{2-} repulsion, reducing the abrupt change of the c-axis during cycling [24]. Moreover, Na^+ ions can maintain the channel open for rapid and smooth Li^+ ion diffusion into the layered structure. Therefore, we can conclude that surface modification via sodium doping can effectively improve structural stability and electrochemical characteristics of Ni-rich cathode materials. Rate performances of the pristine NCM and N-NCM samples are tested at different discharge C-rates between 0.1 C and 2 C. As shown in Fig. 3(b), there is no big difference at low C-rate from 0.1 C to 1.0 C. In contrast, it can be confirmed that the prominent change in the capacity between both samples is observed at the high C-rate of 2.0 C. We can explain that surface modification using sodium is beneficial for superior rate capability originated from improving the electronic conductivity as well as enlarging lattice parameters, deriving form rapid Li-ion kinetic [3]. To further study the effect of sodium doping on the NCM particles, FE-SEM images with a cross-sectional polisher are obtained for both samples. As shown in Fig. 3(c), the pristine NCM particle suffers from intergranular cracks. However, the N-NCM (Fig.

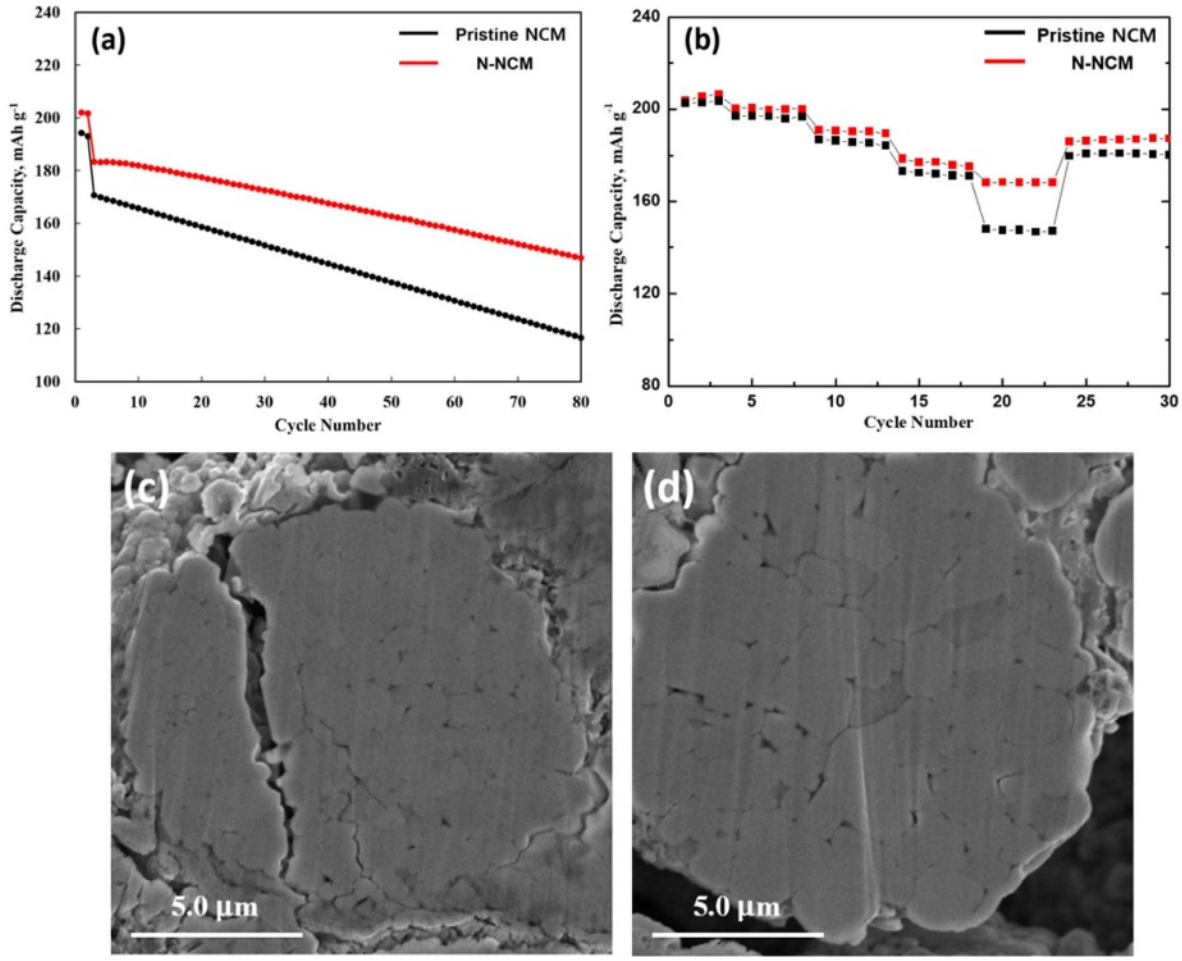

Fig. 3. (a) Cycle performances and (b) rate performance of pristine NCM and N-NCM. Cross-sectional FE-SEM images of (c) pristine NCM and (d) N-NCM.

3(d)) possesses original morphology with the suppression of microcracks.

Conclusions

In summary, we successfully synthesized the Na-doped Ni-rich $LiNi_{0.8}Co_{0.1}Mn_{0.1}O_2$ cathode to enhance the cycling performance. These improvements of Ni-rich NCM cathode are derived from enlarged Li slab spacing, resulting in providing smooth and fast lithium-ion insertion-extraction. The substitution of Na^+ for Li contributes to enhanced structural stability and better electrochemical performances. Therefore, it can be concluded that bulk doping using sodium can be regarded as a promising cathode for high-energy and long-life LIBs.

References

1. S.H. Lee, G.J. Park, S.J. Sim, B.S. Jin, and H.S. Kim, J. Alloys Compd. 791 (2019) 193-199.
2. D.Y. Hwang, S.J. Sim, B.S. Jin, H.S. Kim, and S.H. Lee, ACS Appl. Energy Mater. 4 (2021) 1743-1751.
3. S.J. Sim, S.H. Lee, B.S. Jin, and H.S. Kim, Sci. Rep. 9 (2019) 8952.
4. T. Sattar, S.H. Lee, B.S. Jin, and H.S. Kim, Sci. Rep. 10 (2020) 8562.
5. J. Kim, H. Lee, H. Cha, M. Yoon, M. Park, and J. Cho, Adv. Energy Mater. 8 (2017) 1702028.
6. S.K. Hu, G.H. Cheng, M.Y. Cheng, B.J. Hwang, and R. Santhanam, J. Power Sources 188 (2009) 564-569.
7. S.J. Sim, S.H. Lee, B.S. Jin, and H.S. Kim, Sci. Rep. 10 (2020) 11114.
8. S. Li, X. Fu, J. Zhou, Y. Han, P. Qi, X. Gao, X. Feng, and B. Wang, Chem. Mater. 4 (2016) 5823-5827.
9. L. Xia, K. Qiu, Y. Gao, X. He, and F. Zhou, J. Mater. Sci. 50 (2015) 2914-2920.
10. A. Chen, L. Kong, Y. Shu, W. Yan, W. Wu, Y. Xu, H. Gao, andY. Jin, RSC Adv. 9 (2019) 12656-12666.
11. T. Sattar, S.H. Lee, S.J. Sim, B.S. Jin, and H.S. Kim, Int. J. Hydrog. Energy 45 (2020) 19567-19576.
12. G. Singh, R. Thomas, A. Kumar, R.S. Katiyar, and J. Electrochem. Soc. 159 (2012) A410-A420.
13. M. Choi, S.H. Lee, Y.I. Jung, W.K. Choi, J.K. Moon, J. Choi, B.K. Seo, and S.B. Kim, Trans. Electr. Electron. Mater. 19 (2018) 417-422.
14. K.S. Lee, S.T. Myung, K. Amine, H. Yashiro, and Y.K. Sun, J. Electrochem. Soc. 154 (2007) A971.
15. Y. Liu, S. Shen, J. Zhang, W. Zhong, and X. Huang, Appl. Surf. Sci. 478 (2019) 762–769.

16. K.M. Shaju, G.V.S. Rao, and B.V.R. Chodari, Electrochimica Acta 48 (2002) 145-151.
17. M. wang, R. Zhang, Y. Gong, Y. Su, D. Xiang, L. Chen, Y. Chen, M. Luo, and M. Chu, Solid State Ionics. 312 (2017) 53–60.
18. D. Zeng, J. Cabana, J. Bréger, W.S. Yoon, and C.P. Grey, Chem. Mater. 19 (2007) 6277-6289.
19. S.H. Lee, H.S. Kim, and B.S. Jin, J. Alloy. Comp. 803 (2019) 1032-1036.
20. S.H. Lee, S.J. Sim, and B.S. Jin, H.S. Kim, Sci. Rep. 9 (2019) 8901.
21. Y.Y. Wang, Y.Y. Sun, S. Liu, G.R. Li, and X.P. Gao, ACS Appl. Energy Mater. 1 (2018) 3881-3889.
22. J.W. Seok, J. Lee, T. Rodgers, D.H. Ko, and J.H. Shim, Trans. Electr. Electron. Mater. 20 (2019) 548-553.
23. W. Hua, J. Zhang, Z. Zheng, W. Liu, X. Peng, X.D. Guo, B. Zhong, Y.J. Wang, and X. Wang. Dalton Trans. 43 (2014) 14824.
24. T. Chen, F. Wang, X. Li, X. Yan, H. Wang, B. Deng, Z. Xie, and M. Qu, Appl. Surf. Sci. 465 (2019) 863-870.